Analysis of Article on Kuramoto Model with Positive and Negative Coupling Parameters

Nathan Isaman
Aeronautical and Astronautical Engineering
University of Washington
Seattle, Washington 98105
Email: nisaman@uw.edu

***Abstract*—The purpose of this paper is to review and recreate the simulations in "Kuramoto Model of Coupled Oscillators with Positive and Negative Coupling Parameters: An Example of Conformist and Contrarian Oscillators"[1]. The primary focus of this paper's analysis will be on the initial section of [1] where the steady-state dynamics of the Conformist/Contrarian Kuramoto model is investigated with different parameter values. A discussion of the differences in the recreated simulations and the source simulations, an overview of the remainder of [1], and applications/extensions to this work will also be provided.**

1. Problem Setup and Assumptions

The standard Kuramoto model for the i^{th} coupled oscillator in a network of oscillators is the following differential equation.

$$\dot{\phi}_i = \omega_i + \frac{K}{N}\sum_{j=1}^{N}\sin\left(\phi_j - \phi_i\right) \tag{1}$$

Here, N is equal to the number of agents in the system, ϕ_i and ϕ_j represent the phases of the i^{th} and j^{th} agents respectively, and ω_i represents the natural frequency of the i^{th} agent. The parameter of interest in this paper is the coupling strength coefficient, K. Normally, this value is strictly positive and influences the system's transition to various states of synchronization. In [1], however, each agent was assigned their own value, K_i, and this value was allowed to become negative. The negative valued K_i's would represent contrarian agents in the system, agents that diverge from the prevailing opinion. A positively valued K_i's would then represent a conformist agent, who would tend towards the prevailing opinion. In [1], the value of K_i was drawn from a double-δ distribution:

$$\Gamma(K) = (1-p)\delta(K-K_1) + p\delta(K-K_2) \tag{2}$$

The variable p represents the probability that the i^{th} agent will be a conformist and the two K values, K_1 and K_2, represent the contrarian and conformist coupling strengths respectively. Each $\delta(\cdot)$ represents the Dirac-delta function centered at the respective K_i. The natural frequencies, ω_i, found in (1) were drawn from a Lorentzian distribution with $\mu = 0$ and width γ:

$$g(\omega) = \frac{\gamma}{\pi((\omega-\mu)^2+\gamma^2)} \tag{3}$$

Another important equation that will be used in the analysis of the source paper's findings is the following complex order parameter, Z.

$$Z = Re^{i\Phi} = \frac{1}{N}\sum_{j=1}^{N} e^{i\phi_j} \tag{4}$$

The R represents the system's macroscopic coherence and takes values $0 \leq R \leq 1$ where 0 implies perfect incoherence and 1 implies perfect coherence. The Φ component represents the system's mean phase. Since the underlying graph is assumed to be a complete graph on N nodes, it is clear that the agents in this system will essentially interact via these mean-field parameters R and Φ. Equation (1) can therefore be simplified into the following:

$$\dot{\phi}_i = \omega_i + K_i R\sin\left(\Phi - \phi_i\right) \tag{5}$$

The last parameter of interest for use for this paper is Q. This represents the ratio of the coupling strengths between the conformist and contrarian agents. The higher this value is, the stronger the contrarians are impacted by the conformist values.

$$Q = \frac{-K_1}{K_2} \tag{6}$$

2. Results

Reproducing the dynamics seen in figures 1, 2, and 3 from [1] were the primary objective of the simulations seen in this paper. For ease of reference, these source figures have been added to this paper as Figures 1-3. All credit for these figures belongs to [1]. Figure 1 illustrates two of the three phase-states observed in the conformist/contrarian Kuramoto model. The top subplots (a and b) show the π-state and the bottom subplots (c and d) show the transition wave (TW) state. The π-state is distinguished by a phase-peak separation of π and a set point value for the complex

order parameter Z, when mapped on the complex plane. The TW-state is characterized by a phase-peak separation of less than π and a limit cycled Z value. Please note that these plots are for the steady-state behavior of the system and the preceding transient values have been discarded.

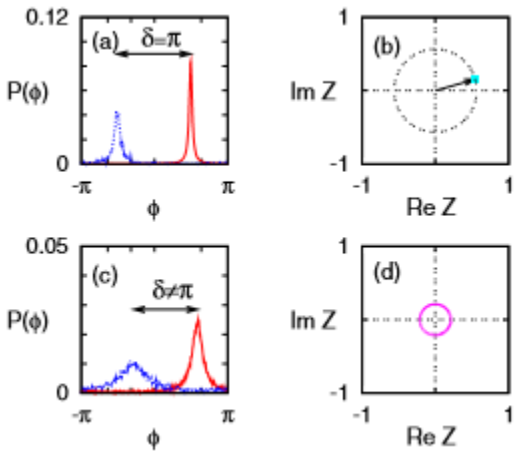

Figure 1. Phase distribution for $\gamma = 0.05$, $N = 25,600$, $K_1 = -0.5$, $K_2 = 1.0$. Source: [1].

2.1. Simulation Set-up

All of the simulations conducted to verify the results of [1] were done in MATLAB using the system parameter values found in the parameters table and with the best numerical implementations of equations (1)-(4) available. Parameter differences between this paper's simulations and those found in [1] will be discussed in section 3.3. Equation (1) was implemented numerically in lieu of equation (5) simply to reduce the computational complexity of the solution. Equation (3) was implemented using $\mu = 0$ and an N-length vector of normally distributed random x values to generate an N-length vector of ω_i's using the equation exactly as shown. The complex order parameter in equation (4) was implemented exactly as shown. The equation from [1] that required some interpretation on how to properly or even approximately implement was equation (2). The Dirac-delta function is zero for all values not equal to K_i and is "infinity" when $K = K_i$, which poses an issue for assigning these values to agents reliably. An N-length vector of K_i's was created where the first Np values were set to K_2 and the remaining $N(1-p)$ values were set to K_1. This ensures that a reliable and consistent proportion of the N agents is assigned to the role of conformist or contrarian depending on the desired p value. This does limit the viable combinations of N and p to those that result in integer values. Numerical integration was performed using *ode45()* in MATLAB with modified code found in [2]. The only major deviation in the functional implementation of (1) is the presence of different K_i values. This difference resulted in only a trivial coding adaptation.

Simulation Parameters		
Parameter / Q	0.5	3.0
γ	0.05	0.05
N	100	100
p	0:0.01:1.0	0:0.01:1.0
K_1	-0.5	-3.0
K_2	1.0	1.0

2.2. Simulation Results

The key results from the recreated simulations can be seen in Figures 4-6 with additional figures available in Appendix 1. The left plot in Figure 4 represents the distribution of phases at steady-state for a p value of 0.63; a majority of conformists. There are two distinct peaks where the conformists and contrarians have congregated and are at a phase-peak separation of less than π. This is also confirmed by the right plot in Figure 4 since the complex order parameter is clearly tracing out a limit cycle with a semi-constant R value. Figure 4 corresponds to the results in Figure 1c and 1d. A few examples corresponding to Figure

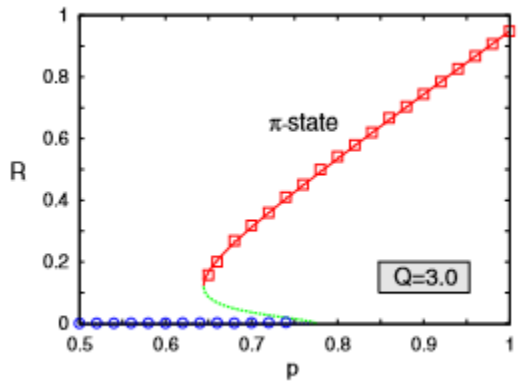

Figure 2. Order Parameter R vs p for Q = 3. $\gamma = 0.05$, $N = 25,600$, $K_1 = -3.0$, $K_2 = 1.0$. Source: [1].

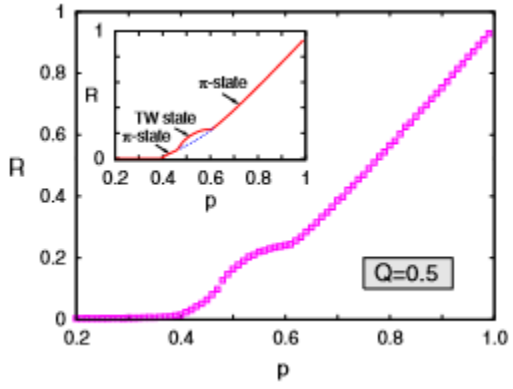

Figure 3. Order Parameter R vs p for Q = 0.5. $\gamma = 0.05$, $N = 25,600$, $K_1 = -0.5$, $K_2 = 1.0$. Inset figure denotes theoretical predictions whereas the outer figure is from simulation results. Source: [1].

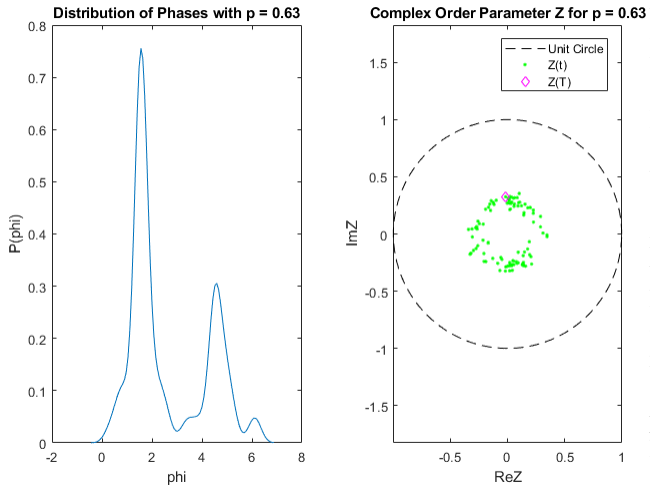

Figure 4. Steady-State Phase distribution for p = 0.63, Q = 0.5. Image shows bimodal distribution of frequencies indicating coherence among conformists and contrarians.

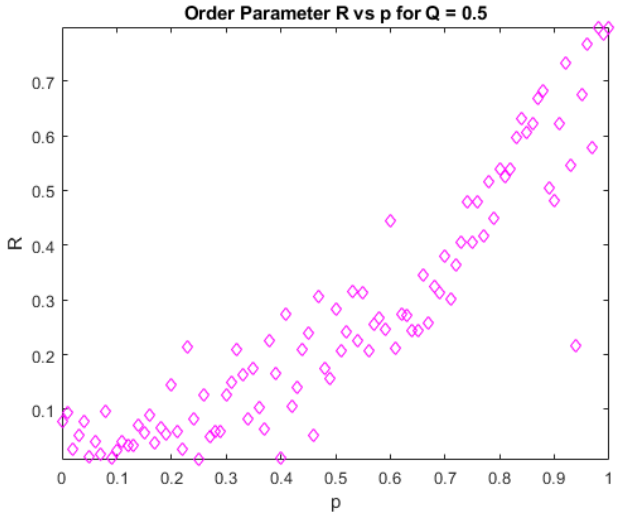

Figure 5. Complex Order Parameter R vs proportion of conformists p for Q = 0.5.

1a and 1b can be found in Appendix 1. It was actually quite challenging to arrive at a semblance of a π-state in the recreated simulations. Potential reasons for this will be discussed in the next subsection.

Figure 5 illustrates the change in the complex order parameter R for a Q of 0.5 as p is varied from 0 to 1.0; as the system goes from containing no conformists to being comprised entirely of them. This figure corresponds to Figure 3 from [1] and has hints of the representative curve seen in Figure 3. The curve hugs the p-axis until around p = 0.4, where it begins its ascent. The TW-state portion from $0.4 \leq p \leq 0.65$ seen in Figure 3 is not as apparent in Figure 5. Nevertheless, there is a small hump in the curve in this region of p values. Figure 4 also represents a system in this region and it exhibits TW-state behavior as discussed above. After crossing past $p = 0.65$, both figures continue linearly upward toward a (p,R) intercept around (1,0.8).

The next simulation comparison is between the results in Figures 2 and 6. These both correspond to Q values of 3.0, where the contrarian agents are much more strongly affected by the conformist agents. The only two features from Figure 2 that are represented in Figure 6 is the extended incoherent region $0.0 \leq p \leq 0.6$. This intuitively makes sense as the contrarians, who comprise most of the system at these levels, are increasingly perturbed by the growing number of conformists until well after the conformists assume the majority. The interesting parabolic curve segment in Figure 2 is completely absent in Figure 6. After this region, both plots continue linearly to approximately the same terminal levels.

The standard Kuramoto model has a single, unique coupling strength, K, for all of the agents in the system. As a result of this, the standard system tends towards stable phase-locked synchronization. The introduction of contrarian agents to this standard model has given rise to the traveling wave state where the mean phase stabilizes, given the appropriate conditions, to a limit cycle. The standard Kuramoto model does not exhibit this behavior. This is a fascinating and dynamic system feature where the contrarian and conformist agents' mean phases push each other around the cycle.

2.3. Sources of Error or Difference

It is clear, from the previous section, that the original and recreated simulations are similar and have most of the same key features. Another notable takeaway was that there were also quite a few differences. The potential causes or rationale for those differences will be discussed in this section. There are a number of instances where the

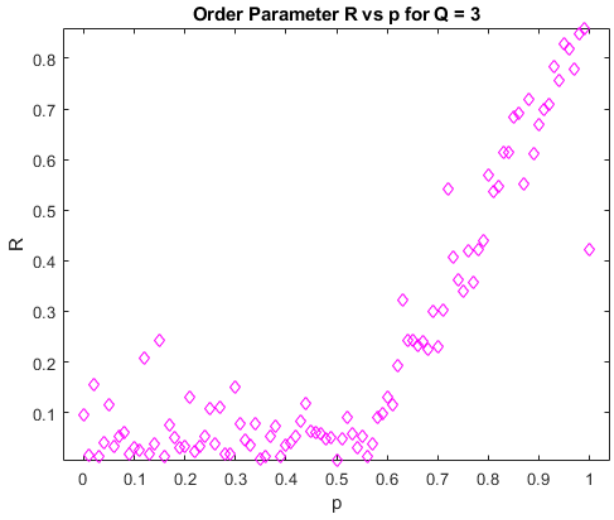

Figure 6. Complex Order Parameter R vs proportion of conformists p for Q = 3.0.

implementation details in [1] were vague or not specified at all. These are the areas where the recreated simulation and source simulation are most likely to diverge. One specific instance of this is the implementation of the $\Gamma(K)$ distribution. It is unclear from the article if these values were pulled from a distribution function or allocated as specified in Section 1 of this paper. The first attempt at implementing the $\Gamma(K)$ function involved using MATLAB's *dirac()* function, but that resulted in a vector of 0's for the K_i's. It was after this failure that the direct, p-proportional allocation of K_i's was implemented. Another certain divergence in methods is how the differential equation was integrated. The authors stated in [1] that they numerically integrated the modified (1) using Heun's method, which is an explicit trapezoidal method for numerical integration. Essentially an improved Euler's method. The simulations conducted for this paper utilized MATLAB's *ode45()*, which is an explicit Runge-Kutte method. The differences in these two methods could greatly impact the outcome of the simulations.

On the topic of numerical integration and computational complexity, there is also the difference in the number of agents used. This paper utilized a system of only 100 agents, whereas the original simulations were run on a system of 25,600 agents. This two order of magnitude difference in agents could definitely change the robustness of the simulation results. While the agents interact with each other via the mean field parameters of R and Φ, there is a certain inertia to these values when the number if agents is high. If there is an outlier agent, who perhaps has a significantly different natural frequency relative to the rest of the system, the mean phase of the N = 25,600 system will be essentially unaffected. The same cannot necessarily be said for the N = 100 system. This might also be the cause of the visible noise seen in Figures 4-6 when compared to Figures 1-3, assuming no filtering was done to the figures in [1]. The rationale for utilizing only 100 agents for the simulations in this paper is purely due to the computational load. A number of simulations were run using N = 5000 and it took approximately one hour for the single simulation to run. The N value was thus decreased to improve simulation turnaround time. The authors of [1] might have a more efficient algorithm or perhaps a significantly more powerful computing platform in order to so accurately simulate so many agents. This is an obvious area of improvement for future simulations efforts.

3. Other Components of Source Article

This paper only recreated and verified the simulations and results from the beginning of [1]. The remainder of the article goes on to provide an analytic foundation or rationale for the numerical findings. The first step the authors took was to reduce the model in (4) to a lower dimensional system that characterizes the macroscopic behavior of the overall system. Through various simplifying assumptions, such as $N \longrightarrow \infty$, and the application of Ott and Antonsen's ansatz, the authors were able to distill the nature of the contrarian/conformist Kuramoto model to the following set of complex order differential equations:

$$\dot{z}_1 = -2\gamma z_1 - Q[(pz_2+(1-p)z_1) - (p\bar{z}_2+(1-p)\bar{z}_1)z_1^2] \quad (7)$$

$$\dot{z}_2 = -2\gamma z_2 - (pz_2+(1-p)z_1) - (p\bar{z}_2+(1-p)\bar{z}_1)z_2^2 \quad (8)$$

This set of equations, according to the authors, is "guaranteed to capture all the long-term macroscopic behavior of the original model" [1]. These equations were then investigated to determine some analytic results regarding the three attractors (incoherence, TW-state, and π-state) and their bifurcation points. They determined that the incoherent state corresponded to the fixed point $(z_1, z_2) = (0, 0)$ and that this state was stable if and only if $p < p_c$ where

$$p_c = \frac{Q+2\gamma}{Q+1} \quad (9)$$

They also determined that the π-state is "born" at this p_c value. The authors also determined that the traveling wave state arises when "the circle of π-states loses stability and turns into a circular limit cycle" for the equations (7) and (8) [1]. Various upper and lower limits are provided in [1] regarding this transition from the stable π-state into the traveling wave state.

4. Applications and Implications

The three phases observed in section 2 provide an interesting insight into the dynamics of a system with a certain proportion of contrarians. When the system is all contrarians, no synchronization of opinion occurs and everyone goes their own way. Harmony is never reached. As this proportion decreases, the contrarians still disrupt the synchronization of the conformists up to the transition wave state. This state, which can almost be commiserated with in the current social/political scene, represents a seemingly stable environment, but the prevailing opinion is constantly changing and the two polarized groups just go in circles. Synchronization never locks onto a set value and the system is therefore in a limit cycle. It is only when the proportion of conformists is notably greater than the contrarians that a more stable synchronization can occur. When the dissenting voices are outnumbered enough that a single set point can be agreed upon and maintained despite minor disruption.

5. Potential Extensions

The implications from the previous section might make it seem like there is no upside to having contrarians in the mix. They only seem to disrupt the system and potentially prevent agreement, after all. The findings in [1] and in section 2 certainly support this for certain ranges of p. An interesting extension to this study would be state or time dependent K_i values. If the coupling strength of the conformists and/or contrarians were proportional to the macroscopic coherence value R, for example. Another potential extension is related to the idea outlined above, with time-varying K's. The system can be composed of conformists

and contrarians, as in this paper and in [1], but with a small cluster of ”insider” agents. These agents would wait until the system has reached steady-state and the nodes are clustered together and in sync, then they would instantaneously change sign and magnitude to become highly repulsive to their tightly packed neighbors. It would be interesting to see if the system would recover to synchronization after this ”betrayal.”

References

[1] Hong, Hyunsuk, and Steven H. Strogatz. ”Kuramoto model of coupled oscillators with positive and negative coupling parameters: an example of conformist and contrarian oscillators.” Physical Review Letters 106.5 (2011): 054102.

[2] Marsh, J. (2008). The Kuramoto Model. [online] Uccs.edu. Available at: https://www.uccs.edu/ jmarsh2/doc/Kuramoto.pdf [Accessed 5 Jun. 2018].

6. Appendix 1: Additional Figures

6.1. Figures for various p values, Q = 0.5

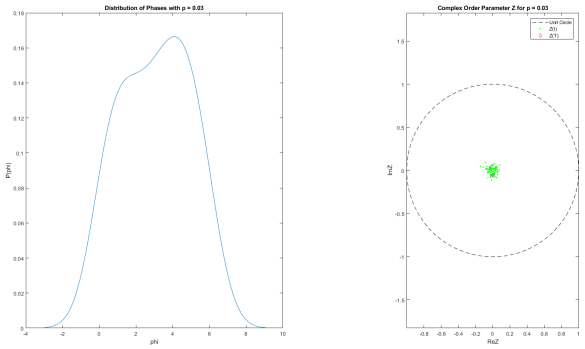

Figure 7. Steady-State Phase distribution for p = 0.03, Q = 0.5. Image shows a semi-normal distribution indicating incoherence.

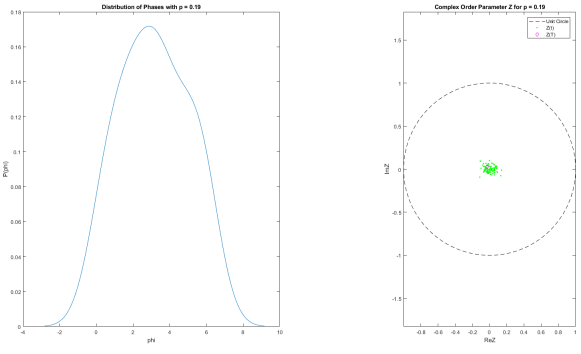

Figure 8.

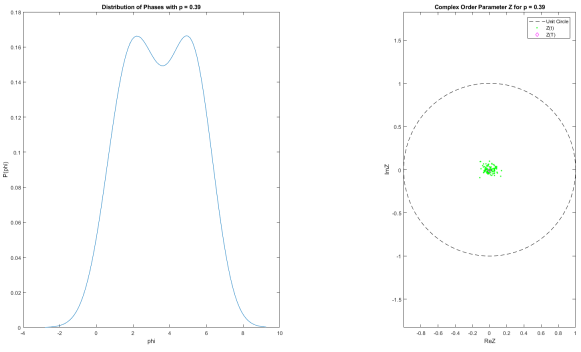

Figure 9.

6.2. Figures for various p values, Q = 3.0

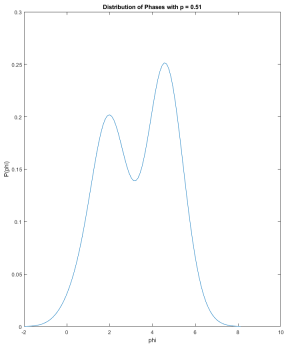

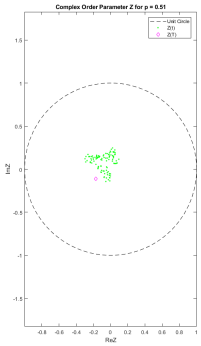

Figure 10.

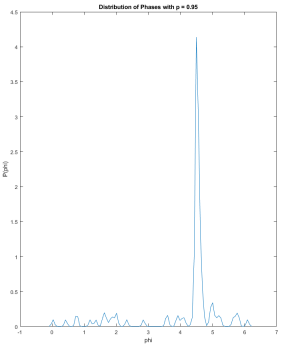

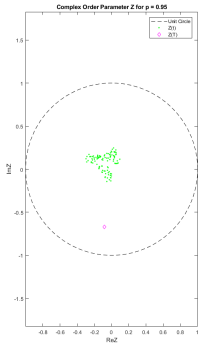

Figure 13.

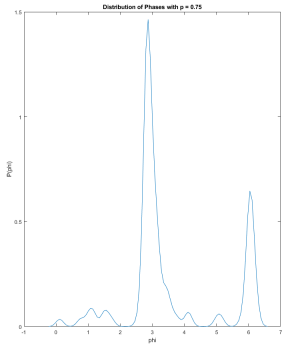

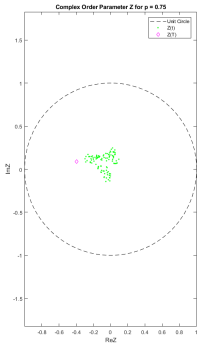

Figure 11.

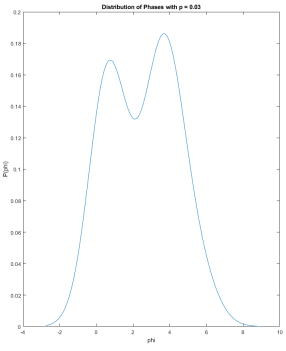

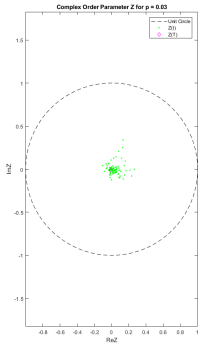

Figure 14.

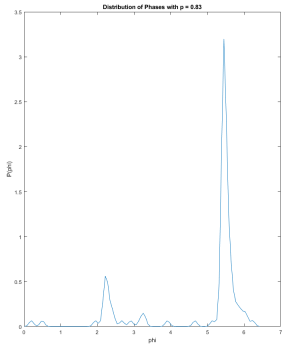

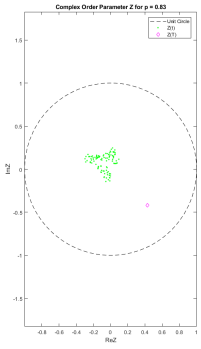

Figure 12.

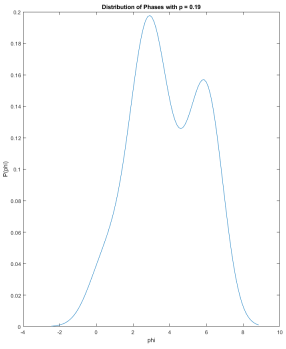

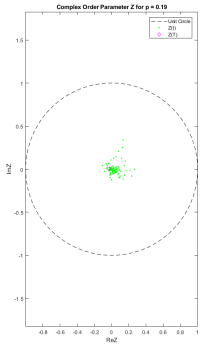

Figure 15.

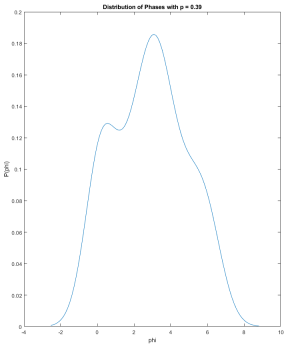

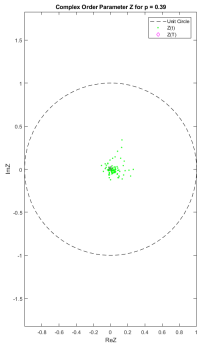

Figure 16.

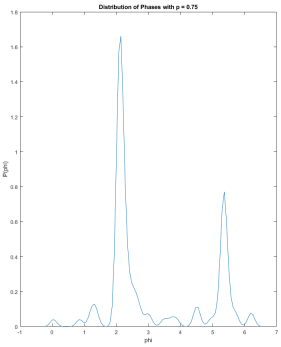

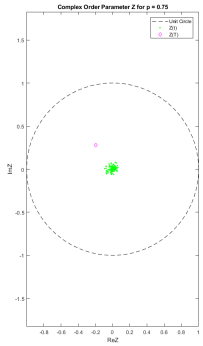

Figure 19.

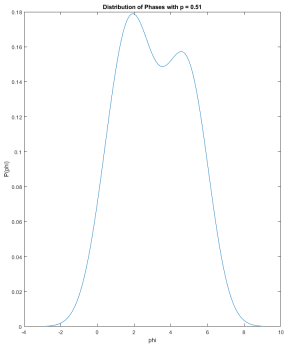

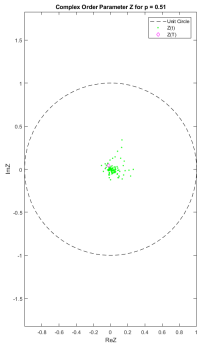

Figure 17.

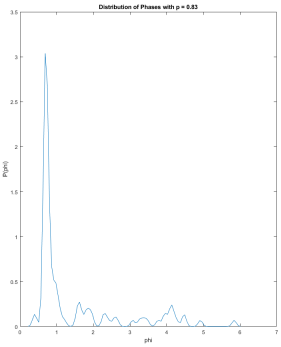

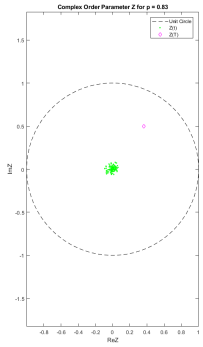

Figure 20.

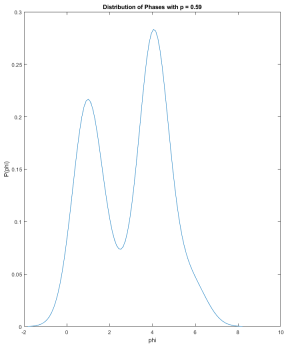

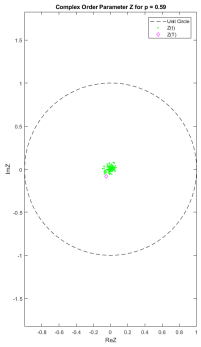

Figure 18.

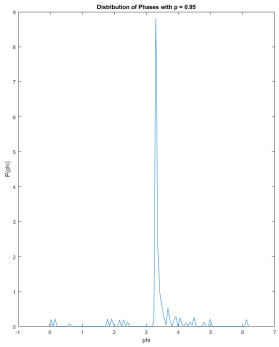

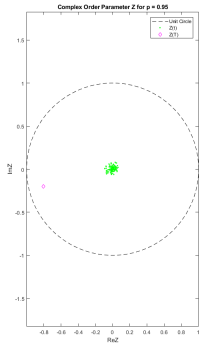

Figure 21.

Kuramoto Model of Coupled Oscillators with Positive and Negative Coupling Parameters: An Example of Conformist and Contrarian Oscillators

Hyunsuk Hong[1] and Steven H. Strogatz[2]

[1]Department of Physics and Research Institute of Physics and Chemistry, Chonbuk National University, Jeonju 561-756, Korea
[2]Department of Mathematics, Cornell University, New York 14853, USA

(Received 2 November 2010; published 2 February 2011)

We consider a generalization of the Kuramoto model in which the oscillators are coupled to the mean field with random signs. Oscillators with positive coupling are ''conformists''; they are attracted to the mean field and tend to synchronize with it. Oscillators with negative coupling are ''contrarians''; they are repelled by the mean field and prefer a phase diametrically opposed to it. The model is simple and exactly solvable, yet some of its behavior is surprising. Along with the stationary states one might have expected (a desynchronized state, and a partially-synchronized state, with conformists and contrarians locked in antiphase), it also displays a traveling wave, in which the mean field oscillates at a frequency different from the population's mean natural frequency.

DOI: 10.1103/PhysRevLett.106.054102 PACS numbers: 05.45.Xt, 89.75.−k

Globally coupled phase oscillators have been used to model diverse self-synchronizing systems in physics, chemistry and biology [1]. In the simplest cases the coupling is uniform: all the oscillators interact with equal strength, as in the classic Kuramoto model

$$\dot{\phi}_i = \omega_i + \frac{K}{N}\sum_{j=1}^{N}\sin(\phi_j - \phi_i), \qquad i = 1, \ldots, N. \quad (1)$$

Here $\phi_i(t)$ is the phase of the ith oscillator at time t, and ω_i is its natural frequency, chosen at random from a unimodal, symmetric probability density $g(\omega)$. Kuramoto assumed the coupling strength K is positive, corresponding to an attractive interaction between the oscillators.

A natural generalization is to allow K to have either sign. There are various ways to do this while still retaining the simplifying assumption of infinite-range interactions [2]. Several authors, inspired by models of spin glasses [3], have examined the effects of replacing K with random positive and negative coupling terms K_{ij} inside the sum in Eq. (1). The matrix elements K_{ij} are usually assumed to be symmetric ($K_{ij} = K_{ji}$) and independently chosen from the same probability distribution. The resulting models show evidence of glassy behavior, but their dynamics are not yet well understood [4].

A second approach, motivated by neural networks with excitatory and inhibitory coupling [5], is to replace K with a random variable K_j inside the sum in Eq. (1), where $K_j > 0$ for excitatory neurons, and $K_j < 0$ for inhibitory neurons. Now the randomness is regarded as an intrinsic property of the oscillators themselves [6], rather than of the interactions between them (as in the glassy models). Thus the interactions between i and j need not be symmetric (unless K_i happens to equal K_j). Somewhat surprisingly, extending the Kuramoto model in this fashion yields nothing qualitatively new; the dynamics turn out to resemble those of the original model [7].

Here we explore a third possibility: we replace K by a random variable K_i outside the sum in Eq. (1). The effect is to endow the oscillators with two kinds of personalities. Those with $K_i > 0$ behave like conformists—they tend to fall in line with whatever rhythm has emerged in the population, whereas those with $K_i < 0$ are repelled by the prevailing rhythm and act like contrarians. In that sense the model is loosely analogous to sociophysical models of opinion formation [8]. It is also reminiscent of other two-population variants of the Kuramoto model, such as those involving two frequency distributions [9] or two levels of attractive coupling [10].

The collective rhythm in the model is quantified by the complex order parameter

$$Z = Re^{i\Phi} = \frac{1}{N}\sum_{j=1}^{N} e^{i\phi_j}, \quad (2)$$

where the amplitude $0 \le R \le 1$ measures the system's macroscopic coherence and Φ is the average phase. Then, by replacing K with K_i, we find that Eq. (1) reduces to

$$\dot{\phi}_i = \omega_i + K_i R\sin(\Phi - \phi_i), \qquad i = 1, \ldots, N. \quad (3)$$

Equation (3) shows that the model retains the mean-field character of the original Kuramoto model; all the oscillators effectively interact only through the mean-field variables R and Φ. Furthermore, the term $K_i R\sin(\Phi - \phi_i)$ highlights the difference between the two types of oscillators; it pulls the conformists toward the collective phase Φ but pushes the contrarians away toward $\Phi + \pi$. The resulting dynamics are a bit more subtle than that, however, because the nonidentical frequencies ω_i also play a crucial role.

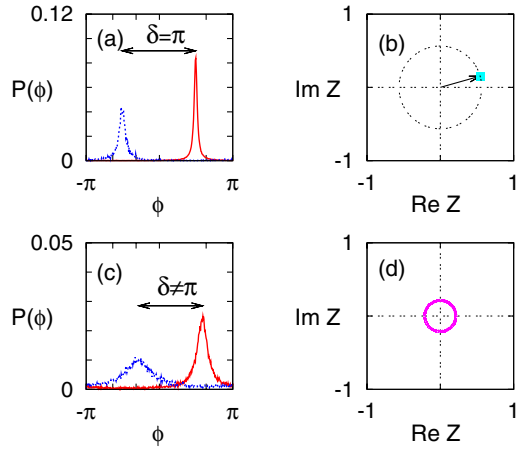

FIG. 1 (color online). The π state and traveling wave state. Parameters: $N = 25\,600$, $\gamma = 0.05$, $K_1 = -0.5$, $K_2 = 1.0$. (a) Phase distribution for the π state; the mean phase difference δ between the conformist (red) and contrarian (blue) oscillators is given by $\delta = \pi$. (b) The order parameter $Z(t)$ for the π-state corresponds to a fixed point. (c) Phase distribution for the traveling wave (TW) state; $\delta \neq \pi$. (d) The order parameter for the traveling wave state traces a circle, implying a nonzero mean phase velocity $\langle \dot{\phi}(t) \rangle \neq 0$.

To probe the system's long-term behavior, we performed numerical simulations. The ω_i were chosen at random from a Lorentzian probability density $g(\omega) = \gamma/[\pi(\omega^2 + \gamma^2)]$ of width γ and mean $\langle \omega \rangle = 0$ (the mean can be set to zero by choosing a suitable rotating frame). For simplicity we assumed a double-δ distribution of coupling strengths: $\Gamma(K) = (1 - p)\delta(K - K_1) + p\delta(K - K_2)$, where $K_1 < 0$ and $K_2 > 0$ represent the couplings for the contrarians and conformists, respectively, and p denotes the probability that a random oscillator is a conformist. Equation (3) was integrated using Heun's method with a time step $\delta t = 0.01$ for 10^5 time steps. The initial 90% of each run was discarded as a transient, after which all quantities of interest were measured.

The system always settles into one of three kinds of long-term behavior, depending on the parameters and initial conditions: (i) *Incoherent state*: The oscillators are completely desynchronized and scattered uniformly across all phases. (ii) *π-state*: The conformist oscillators converge to a partially synchronized state [1], as do the contrarian oscillators. Both generate stationary distributions of phases. The peaks of the distributions, as one would expect, are diametrically opposed, separated by an angle $\delta = \pi$, as shown in Fig. 1(a). Because both distributions are stationary, the order parameter $Z(t)$ remains motionless when plotted in the complex plane [Fig. 1(b)]. (iii) *Traveling wave state*: The phase distributions spontaneously travel at constant speed along the phase axis, always maintaining a constant separation $\delta \neq \pi$ [Fig. 1(c)]. As a result, the order parameter $Z(t)$ traces a circle about the origin at constant angular velocity, as shown in Fig. 1(d).

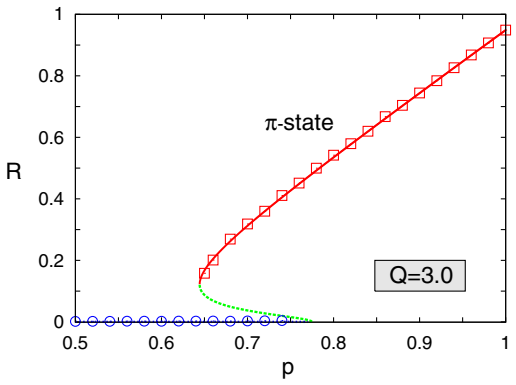

FIG. 2 (color online). Order parameter R vs p for $Q = 3$, computed by numerical integration (symbols) and compared to theoretical prediction from Eq. (11) (lines). Solid lines, stable states; dotted line, unstable π state. Stable π states were found numerically by integrating from the in-phase initial condition $\phi_i(0) = 0$ for all i, for each p. Stable incoherent states were found by integrating from random initial conditions. Parameters: $N = 25600$, $\gamma = 0.05$, $K_1 = -3.0$, $K_2 = 1.0$.

Figs. 2 and 3 show the transitions among these states as we vary p (the proportion of conformists). The results divide into two cases, depending on whether the conformists or the contrarians are more strongly affected by the mean field.

Figure 2 shows what happens when the contrarians are more strongly affected, in the sense that $Q \equiv -K_1/K_2 > 1$. As we increase p from 0, the system starts out incoherent, which makes intuitive sense: for small p, the system is dominated by contrarians who (of course) cannot agree on anything. But once p exceeds a certain threshold, there are enough conformists around for a consensus to emerge. At that point the system jumps discontinuously up to the π state, where it is polarized into two camps. Whatever the conformists decide on, the contrarians

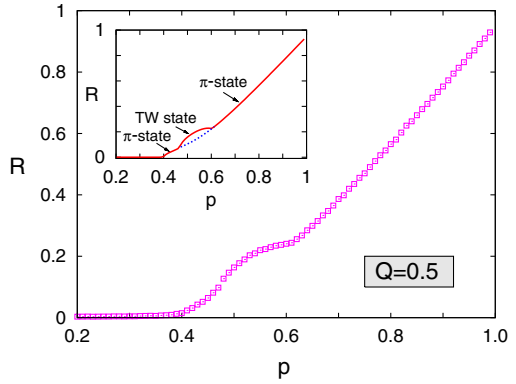

FIG. 3 (color online). Order parameter R vs p for $Q = 0.5$, computed by numerical integration. Inset shows theoretical prediction from Eq. (11). Red solid line, stable states; blue dotted line, unstable state. Parameters: $N = 25\,600$, $\gamma = 0.05$, $K_1 = -0.5$, $K_2 = 1.0$.

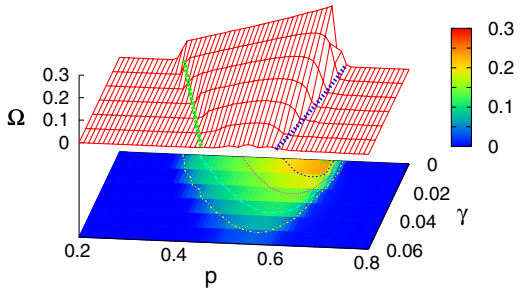

FIG. 4 (color online). Wave speed Ω as a function of γ and p for $Q = 0.5$. The data are also plotted as a contour map, with heights indicated by the color bar. Dotted lines show the predicted transition curves at which the traveling wave is born, as obtained from Eq. (15).

oppose them. Lowering p then yields a discontinuous and hysteretic return to the incoherent state.

On the other hand, if the conformists are more intensely influenced by the mean field ($Q < 1$), the transitions become continuous and reentrant. Figure 3 shows that as p increases from 0, the system goes from incoherence to the π state, then to the traveling wave state and finally back to the π state.

The traveling wave state does not occur in the original Kuramoto model (the limiting case for which $p = 1$) [11] or in the opposite limit $p = 0$ where all the interactions are repulsive [13]. Traveling waves appear only in an intermediate range of p, indicating that both types of oscillators are essential, and only if γ is sufficiently small, indicating that the oscillators need to be close enough to identical. To quantify this, Fig. 4 plots the wave speed $\Omega \equiv (1/N) \times \sum_{j=1}^{N} \langle \dot{\phi}_j \rangle_t$ as a function of p and γ. Notice that the traveling wave state occurs in a wider window as γ tends to 0.

To explain these numerical findings, we begin by reducing the model to a low-dimensional system that governs its long-term macroscopic behavior. As $N \to \infty$, the evolution of the system is given by the continuity equation for the probability density function $f(\phi, K, \omega, t)$:

$$\frac{\partial f}{\partial t} + \frac{\partial}{\partial \phi}(fv) = 0. \tag{4}$$

Here, $v = v(\phi, K, \omega, t)$ is the continuum limit of Eq. (1):

$$v = \omega + K \int \sin(\phi' - \phi) f(\phi', K', \omega', t) \times \Gamma(K') dK' d\phi' d\omega'. \tag{5}$$

The complex order parameter becomes $Z(t) = \int e^{i\phi'} f(\phi', K', \omega', t) \Gamma(K') dK' d\phi' d\omega'$, and the velocity v simplifies to

$$v = \omega + \frac{K}{2i}(Ze^{-i\phi} - \bar{Z}e^{i\phi}), \tag{6}$$

where the overbar indicates the complex conjugate (c.c.). Next we use the remarkable ansatz recently discovered by Ott and Antonsen [14]. The special family of density functions given by

$$f(\phi, K, \omega, t) = \frac{g(\omega)}{2\pi}\left\{1 + \left[\sum_{n=1}^{\infty} [a(K, \omega, t)]^n e^{in\phi} + \text{c.c.}\right]\right\} \tag{7}$$

solves the governing equations exactly, as long as a evolves according to

$$\dot{a} = -i\omega a + \frac{K}{2}(\bar{Z} - Za^2). \tag{8}$$

(This can be checked by substituting Eqs. (6) and (7) into Eq. (4).) Meanwhile, Z reduces to $Z(t) = \int_{-\infty}^{\infty} \int_{-\infty}^{\infty} \Gamma(K) \bar{a}(K, \omega, t) g(\omega) d\omega dK$ since only $n = 1$ in the c.c. term of f contributes to the ϕ integral. A further reduction occurs because $g(\omega)$ is Lorentzian; by closing the contour for the ω integral in the lower half plane, we find $Z(t) = \int_{-\infty}^{\infty} \Gamma(K) \bar{a}(K, -i\gamma, t) dK$. Next, let $z(K, t) = a(K, -i\gamma, t)$. Then Eq. (8) gives

$$\dot{z} = -\gamma z + \frac{K}{2}(\bar{Z} - Zz^2), \tag{9}$$

where $Z = \int_{-\infty}^{\infty} \Gamma(K) \bar{z}(K, t) dK$. For the double-delta distribution $\Gamma(K) = (1 - p)\delta(K - K_1) + p\delta(K - K_2)$, Z is simply

$$Z = (1 - p)\bar{z}_1 + p\bar{z}_2, \tag{10}$$

where $z_1 = z(K_1, t)$ and $z_2 = z(K_2, t)$. The variables z_1 and z_2 have nice interpretations: they are complex order parameters for the contrarians and conformists. From Eqs. (9) and (10), they evolve according to

$$\begin{aligned} \dot{z}_1 &= -2\gamma z_1 - Q[(pz_2 + qz_1) - (p\bar{z}_2 + q\bar{z}_1)z_1^2], \\ \dot{z}_2 &= -2\gamma z_2 + (pz_2 + qz_1) - (p\bar{z}_2 + q\bar{z}_1)z_2^2, \end{aligned} \tag{11}$$

where $q = 1 - p$. (For convenience we have also rescaled time; t has been replaced by $K_2 t/2$ and γ by γ/K_2).

The low-dimensional system (11) is guaranteed to capture all the long-term macroscopic behavior of the original model. This follows from a recent theorem of Ott and Antonsen [15], which makes crucial use of the assumption that the oscillators are nonidentical [16]. We have numerically explored the dynamics of z_1 and z_2 by integrating Eq. (11), and find that we can quantitatively reproduce all the findings shown in Figs. 1–4.

The reduced system yields a number of exact results about the three attractors and their bifurcation points. The incoherent state corresponds to the fixed point $z_1 = 0$, $z_2 = 0$. Linearizing (11) about this state shows that incoherence is stable if and only if $p < p_c$, where

$$p_c = \frac{Q + 2\gamma}{Q + 1}. \tag{12}$$

The π-state is born at p_c when incoherence loses stability and gives rise to a circle of fixed points with $R > 0$. All of these are π-states. They are all equivalent, because of the model's rotational symmetry; they differ only by the arbitrary angle Φ, the phase of the complex order parameter. To calculate how they depend on parameters, let $Z = R > 0$, $z_1 < 0$ and $z_2 > 0$, without loss of generality. Solving Eq. (10) for p, we find $p = (R - z_1)/(z_2 - z_1)$. Then the relevant fixed points of Eq. (11) are $z_1 = [\gamma - \sqrt{\gamma^2 + (QR)^2}]/(QR)$ and $z_2 = (-\gamma + \sqrt{\gamma^2 + R^2})/R$. Hence

$$p = \frac{QR^2 - \gamma + \sqrt{\gamma^2 + (QR)^2}}{-\gamma Q + Q\sqrt{\gamma^2 + R^2} - \gamma + \sqrt{\gamma^2 + (QR)^2}}. \quad (13)$$

This gives an exact parametrization of the π-states. Near the transition point where $R \to 0$, we find that $R \sim (p - p_c)^{1/2}$, where $p_c = (Q + 2\gamma)/(Q + 1)$ as before.

The traveling wave state is created when the circle of π-states loses stability and turns into a circular limit cycle for Eq. (11). To calculate this bifurcation, let $z_1 = r_1 e^{-i\psi_1}$ and $z_2 = r_2 e^{-i\psi_2}$. Then Eq. (11) yields

$$\begin{aligned} \dot{r}_1 &= -2\gamma r_1 - Q(1 - r_1^2)(q r_1 + p r_2 \cos\delta), \\ \dot{r}_2 &= -2\gamma r_2 + (1 - r_2^2)(p r_2 + q r_1 \cos\delta), \\ \dot{\delta} &= \sin\delta\left[Qp\frac{r_2}{r_1}(1 + r_1^2) - q\frac{r_1}{r_2}(1 + r_2^2)\right], \end{aligned} \quad (14)$$

where $\delta \equiv \psi_1 - \psi_2$. The advantage is that the traveling wave state reduces to a fixed point of (14), with $\delta \neq \pi$. Linearizing (14) about the π-state (13) and seeking a zero eigenvalue, we find that for $\gamma \ll 1$ the transition to the traveling wave state occurs at

$$\begin{aligned} p_\ell &= \frac{Q}{1 + Q} + \frac{3\gamma}{1 + Q} + O(\gamma^{3/2}), \\ p_u &= \frac{1}{1 + Q} - \frac{\gamma}{1 + Q} + \frac{(Q + 1)\gamma^2}{(Q - 1)Q} + O(\gamma^3), \end{aligned} \quad (15)$$

where p_ℓ and p_u represent the lower and upper values at which the π state loses stability. These predicted stability boundaries, shown as dotted curves in Fig. 4, are in good agreement with the simulation results. The theory also correctly predicts that if γ is large enough, the traveling wave state disappears and π state becomes stable for all R. For instance, when $Q = 0.5$, a numerical eigenvalue computation shows that the π state is always stable if $\gamma \gtrsim 0.06$, as in Fig. 4.

In future work, it will be interesting to see if the traveling wave also occurs in models with local coupling. Its existence in the present model is made possible by the asymmetry of the coupling: $K_{ij} \neq K_{ji}$. Such asymmetry is common in biological and social systems. For experimental tests of the model's predictions, however, it might be more promising to look for physical realizations of Eq. (3) in series arrays of Josephson junctions [19] or in liquid crystal spatial light modulators suitably coupled by global optoelectronic feedback [20].

Research supported by the LG YONAM Foundation (H. H.) and NSF Grant CCF-0835706 (S. H. S.). We thank R. Roy and K. Wiesenfeld for their helpful comments.

[1] A. T. Winfree, *The Geometry of Biological Time* (Springer, New York, 1980); Y. Kuramoto, *Chemical Oscillations, Waves, and Turbulence* (Springer, Berlin, 1984); J. A. Acebron *et al.*, Rev. Mod. Phys. **77**, 137 (2005).
[2] H. Daido, Prog. Theor. Phys. **77**, 622 (1987); Phys. Rev. Lett. **68**, 1073 (1992); L. L. Bonilla *et al.*, J. Stat. Phys. **70**, 921 (1993); D. H. Zanette, Europhys. Lett. **72**, 190 (2005).
[3] D. Sherrington and S. Kirkpatrick, Phys. Rev. Lett. **35**, 1792 (1975).
[4] J. C. Stiller and G. Radons, Phys. Rev. E **58**, 1789 (1998); H. Daido, Phys. Rev. E **61**, 2145 (2000); J. C. Stiller and G. Radons, Phys. Rev. E **61**, 2148 (2000).
[5] C. Börgers and N. Kopell, Neural Comput. **15**, 509 (2003).
[6] G. H. Paissan and D. H. Zanette, Physica (Amsterdam) **237D**, 818 (2008).
[7] H. Hong and S. H. Strogatz (to be published).
[8] S. Galam, Physica (Amsterdam) **333A**, 453 (2004); M. S. Lama, J. M. López, and H. S. Wio, Europhys. Lett. **72**, 851 (2005).
[9] E. A. Martens *et al.*, Phys. Rev. E **79**, 026204 (2009).
[10] D. M. Abrams, R. Mirollo, S. H. Strogatz, and D. A. Wiley, Phys. Rev. Lett. **101**, 084103 (2008).
[11] Traveling waves were previously seen in a variant of the Kuramoto model where a phase shift term breaks the odd symmetry of the original sine coupling function [12]. In contrast our model retains the odd symmetry, so the traveling waves come in symmetric pairs, with frequencies $\pm\Omega$. They stem from the asymmetry in the coupling parameters K_i, not in the coupling function itself.
[12] H. Sakaguchi and Y. Kuramoto, Prog. Theor. Phys. **76**, 576 (1986).
[13] L. S. Tsimring, N. F. Rulkov, M. L. Larsen, and M. Gabbay, Phys. Rev. Lett. **95**, 014101 (2005).
[14] E. Ott and T. M. Antonsen, Chaos **18**, 037113 (2008).
[15] E. Ott and T. M. Antonsen, Chaos **19**, 023117 (2009).
[16] The theorem does not apply when $\gamma = 0$. The identical case displays states not described by the ansatz above, such as a large manifold of neutrally stable states [17], as seen in other systems [18].
[17] H. Hong and S. H. Strogatz (to be published).
[18] A. Pikovsky and M. Rosenblum, Phys. Rev. Lett. **101**, 264103 (2008); S. A. Marvel and S. H. Strogatz, Chaos **19**, 013132 (2009).
[19] K. Wiesenfeld, P. Colet, and S. H. Strogatz, Phys. Rev. E **57**, 1563 (1998).
[20] E. A. Rogers *et al.*, Phys. Rev. Lett. **93**, 084101 (2004).

```
%% AA 597 - Project - Nathan Isaman
clear all; close all; clc

cases = 0:0.01:1.0;

N = 100;        % Number of agents
g = 0.05;       % Width of Lorentzian distribution
xs = randn(N,1);
ws = lorentzian(xs,0,g);        % Same initial condition for every run

for q = 1:length(cases)

%p = 0.95;
p = cases(q);
K1 = -0.5;
K2 = 1.0;
Q = -K1/K2;
Ki = GammaK2(xs,p,K1,K2);

h = 0.01;
T = 10000;
time = 0:h:T;
%phi_init = (pi/4)*randn(N,1);
phi_init = zeros(N,1);
phi(:,1) = phi_init;
c = Ki/N;
% An alternative approach to calculating the Kuramoto Dynamics:=========
% Src: https://www.uccs.edu/~jmarsh2/doc/Kuramoto.pdf
%fprintf('Starting ode45 on Kuramoto Dynamics...')
dPdt = @(P,W,c)(W+c.*sum(sin(meshgrid(P)-meshgrid(P)'),2));
[times phases] = ode45(@(t,p)dPdt(p,ws,c),[0 T],phi_init);
phi = transpose(phases);
time = transpose(times);
%fprintf('\node45 Complete.')
%=========================================================================
% Forward Euler approach to solving DE (Not very efficient) ============
% for i = 1:length(time)-1
%     for j = 1:N
%         phi(j,i+1) = phi(j,i) + h*kuramoto2(ws(j,1),Ki(j,1),N,phi(j,i),phi(:,i));
%     end
% end
%=========================================================================
% Normalizing the phase wrt Pi (i.e. pushing the phases onto the interval [-pi,pi]
phinorm = zeros(size(phi));
for k = 1:size(phi,2)
    phinorm(:,k) = wrapTo2Pi(phi(:,k));
end
% Plotting ================================================================

% Plotting the Complex Order Parameter (with unit circle shown)
for o = 1:length(phinorm)
```

```
    Zt(o) = complexOrderParam(N,phinorm(:,o));
    ReZt(o) = real(Zt(o));
    ImZt(o) = imag(Zt(o));
end

Zfinal = complexOrderParam(N,phinorm(:,end))
Rfinal = abs(Zfinal)
Rtest(q) = Rfinal;              % Storing R for p vs R plot
ReZ = real(Zfinal);
ImZ = imag(Zfinal);
circlePlot = 1*exp(sqrt(-1)*(0:0.01:2*pi));
ReCir = real(circlePlot);
ImCir = imag(circlePlot);

% Plotting every other p value
if mod(q,4) == 0
    [fd,xd] = ksdensity(phinorm(:,end));
    figure
    subplot(1,2,1)
    plot(xd,fd)
    ylabel('P(phi)')
    xlabel('phi')
    title(['Distribution of Phases with p = ' num2str(p)])

    subplot(1,2,2)
    plot(ReCir,ImCir,'k--'), hold on
    plot(ReZt(end-100:end),ImZt(end-100:end),'g.')
    plot(ReZ,ImZ,'md')
    legend('Unit Circle','Z(t)','Z(T)')
    xlabel('Re{Z}')
    ylabel('Im{Z}')
    title(['Complex Order Parameter Z for p = ' num2str(p)])
    axis equal
    hold off
end
end

figure
plot(cases,Rtest,'md')
title(['Order Parameter R vs p for Q = ' num2str(Q)])
xlabel('p')
ylabel('R')
axis equal
%=========================================================================
%---------------------------Functions-------------------------------
%=========================================================================
function w = lorentzian(x,m,g)
% Function used to generate natural frequencies out of the Lorentzian
% Distribution.
% P(x) = (1/pi)*g/((x-m)^2 + g^2)
% Params:
```

```
% g : distribution mean width
% m : distribution mean; for this case we are assuming m = 0
% x : value at which to evaluate P(x); generally a random number
w = zeros(length(x),1);
for i = 1:length(x)
    w(i,1) = (1/pi)*g/((x(i)^2 + g^2));
end
end

function pdot = kuramoto(wi,Ki,N,phi_i,phis)
% This function represents the RHS of the Kuramoto dynamics
% phi_i_dot = wi + (Ki/N)sum(sin(phi_j - phi_i) for i = 1,...,N
% Params:
% wi : ith agent's natural frequency
% Ki : ith agent's coupling strength
% N  : number of agents in swarm
% phi : the agent's phase

pdot = wi + (Ki/N)*sum(sin(phis - phi_i));
end

function pdot = kuramoto2(wi,Ki,N,phi_i,phis)
% Implementation of equation (3) where the oscillators interact via the
% mean-field variables R and PHI.
PHI = mean(phis);      % Collective/Mean Phase
Z = complexOrderParam(N,phis);
R = real(Z);
pdot = wi + Ki*R*sin(PHI - phi_i);
end


function Z = complexOrderParam(N,phis)
% This function calculates the Complex Order Parameter:
% Z = R*e^(iPHI) = 1/N * SUM(e^i*phi_j)
im = sqrt(-1);
Z = (1/N)*sum(exp(im*phis));
end

function Ki = GammaK(x,p,K1,K2)
% This function represents the double-delta distribution for oscillator
% coupling strengths.
% Ki(x) = (1-p)*dirac(x - K1) + p*dirac(x - K2)
% Params:
% x : point to draw Ki from in the distribution (random entry)
% p : probability that a random oscillator is a conformist
% K1 : coupling strength for contrarian agent
% K2 : coupling strength for conformist agent
vals = rand(length(x),1);

Ki = zeros(length(x),1);
for i = 1:length(x)
```

```
    if vals(i) <= p
        Ki(i,1) = K2;
    end
    if vals(i) > p
        Ki(i,1) = K1;
    end
end
end

function Ki = GammaK2(x,p,K1,K2)
% This function represents the double-delta distribution for oscillator
% coupling strengths.
% Ki(x) = (1-p)*dirac(x - K1) + p*dirac(x - K2)
% Params:
% x : point to draw Ki from in the distribution (random entry)
% p : probability that a random oscillator is a conformist
% K1 : coupling strength for contrarian agent
% K2 : coupling strength for conformist agent
thresh = length(x)*p;
Ki = zeros(length(x),1);
for i = 1:length(x)
    if i <= thresh
        Ki(i,1) = K2;
    end
    if i > thresh
        Ki(i,1) = K1;
    end
end
end
```